Self-consistent charge density and surface electronic states for the (001) face of lithium*

Gerald P. Alldredge and Leonard Kleinman
Department of Physics, University of Texas, Austin, Texas 78712
(Received 13 February 1974)

The self-consistent electronic energy band structure of a 13-layer (001) film of lithium has been calculated using the method described previously. The crystalline potential is described in terms of a nonlocal pseudopotential, with exchange-correlation effects treated in terms of the local approximation used in the Lang-Kohn jellium studies. The planar averages of both charge density and local part of the potential exhibit Friedel oscillations that are appreciably greater than a superposition of the jellium results on the bulklike envelopes in the inner selvage region; in the outer selvage the planar average of the potential agrees well with the jellium result. The (unoccupied) surface state appearing in the $\bar{X}$ gap of the two-dimensional band structure in our initial communication has descended almost to the bulk band below, and in its place a surface state of complementary planar symmetry has descended into the $\bar{X}$ gap from the bulk band above.

I. INTRODUCTION

In a recent paper[1] (hereafter referred to as AK) we presented a method for calculating the energy bands of thin films with free surfaces. The method has the advantage that the potential varies continuously from the interior of the film out into the vacuum regions, and it can be made self-consistent. To illustrate the method, AK presented the results of a band calculation over the surface Brillouin zone (SBZ) of a 13-layer Li (001) film, for which the potential was taken as a superposition of atomic pseudopotentials. Those results verified the insight—drawn partially from phonon calculations for thin films[2]—that, even for ultrathin films of a dozen or so atomic layers, surface-localized excitations characteristic of essentially infinitely thick films can be resolved out of the size effects.[3] The potential used in AK, however, was nowhere near self-consistent in the surface region, so that the details of the results in AK, e.g., the character of the surface state, had to be regarded as preliminary. The present paper reports the results of carrying our method to self-consistency for the 13-layer Li (001) film.

To place the present work in perspective, we might characterize it and the recent work by Appelbaum and Hamann[4] (hereafter referred to as AH) as marking the first realistic confluence of what has heretofore been two equally old, but largely separate streams of development in the theory of electronic structure of crystalline surfaces, particularly those of metals.[5] One stream has been the analysis of the interacting inhomogeneous electron gas for which the nuclei are treated in lowest order as a smeared-out uniform background of neutralizing positive charge ("jellium model"). In the more advanced work, the effects of the discrete lattice on energies such as surface energy and work function are entered as corrections via the use of pseudopotentials in perturbation theory. An extensive review of this area has just been given by Lang.[6] The other stream of development is marked by an emphasis on the interactions between the conduction electrons and the ionic lattice and on the ways in which the termination (and other modifications) of the crystal potential at a surface can give rise to localized or quasilocalized surface states. A major difficulty with this approach has always been the crucial question: What *is* the modification of the crystal Hamiltonian at a surface? The full answer to that question involves not only the self-consistent solution of the electron system in a fixed bulklike array of ions ("level one of self-consistency"), but also the self-consistent solution which allows the array of ions in the surface region to relax from their bulklike positions to new equilibrium positions which may even change the planar symmetry of the surface and which may vary greatly with temperature ("level 2 of self-consistency"). In the absence of such an answer, it is not surprising that the problem of surface states has been subjected to a multitude of model calculations in which the content of physical reality ranges from irrelevant and even misleading to fairly good; we refer the reader to two recent reviews[7] for discussion and evaluation of this body of work and for further references.

Since the methods presented in AK and AH achieve results in somewhat different and complementary ways, we think it useful to devote the remainder of this section to an overview of the major points of similarity and difference. Both methods are similar in their applications to nearly-free-electron (NFE) crystals in that pseudopotentials are used to treat the electron-ion interaction at a level of realism approaching that of current stan-

dards of practice for bulk band-structure calculations. Both treat the electron-electron interactions at a level approaching that of the best current work on the inhomogeneous electron gas near a jellium surface.[6,8] (Our treatment of exchange and correlation as described below is a bit more explicit than AH.) In carrying the methods to self-consistency, neither has been taken beyond level one; the far more difficult level two of self-consistency remains a future goal. The similarity between our work and AH, as applied to NFE metals, persists up to the expandion of the (pseudo) wave function in a basis of two-dimensional plane waves (2DPW's) to account for the translational symmetry of the surface. For local pseudopotentials, used by AH, the one-electron Schrödinger equation in this mixed representation becomes a set of coupled ordinary differential equations in the remaining spatial coordinate z (normal to the surface), each member of the set belonging to a given 2DPW. AH then numerically integrate this set of coupled equations between the vacuum region and a matching plane two or three atomic planes deep into the crystal where the integrated wave functions are matched to bulk-wave functions. Since the principal focus of AH is on the self-consistent charge density near the surface, they do not investigate individual states; indeed their calculation explicitly omits consideration of the evanescent waves of the bulk-band structure which would have to be matched to surface-state wave functions (this omission is not essential to their method and has been lifted in a subsequent paper[9]). Because the step-wise integration of a small set of coupled linear differential equations is a relatively fast procedure, in terms of computer time required, the AH method is very quick.

In Sec. II we describe our method in some detail, but here we briefly summarize the important points of contrast with the AH method. Since we are interested in the band structure of the thin film, we focus on the high-symmetry points and lines of the SBZ, where the 2DPW's are collected into symmetrized 2DPW's transforming according to the various irreducible irrepresentations of the groups of the planar wave vectors $\bar{k}$. The remaining z variation of the Schrödinger equation is expanded in a set of basis functions that approximate the vanishing of the electron wave functions in the vacuum region, so that the Schrödinger equation becomes a matrix eigenvalue equation. Thus, unlike AH our method can as easily accomodate nonlocal potentials as local potentials. Indeed, for Li which has no p-like components in the repulsive part of its pseudopotential, a nonlocal potential is greatly preferred[10] and we use such a potential in AK and the present work. Furthermore, the solution of the matrix-eigenvalue equation of the thin film for the negative eigenvalues yields the *complete* band spectrum of the film—surfacelike and bulklike levels together—without intermediate steps such as calculating evanescent waves of the bulk and matching procedures. These intermediate steps introduce the possibility of inadvertent errors, and a thin-film calculation such as ours provides a valuable independent check. To illustrate the nontriviality of this point, we cite our collaboration with Caruthers in a series of thin-film calculations for aluminum[11] which yielded surface states which were apparently missed in an earlier evanescent-wave-matching calculation.[12] The occupied surface states of crystals are of obvious interest. Even the surface state levels lying between the Fermi level and the vacuum level (which are the only surface states found in the monovalent NFE metals) are of interest in that they are indicators of the crystal potential near the surface; Lundquist *et al.*[13] have recently proposed a combined photo- and field-emission experiment that can probe such unoccupied surface states. As a final point, we note that thin-film calculations such as these can answer questions of interest for thin films *per se*, e.g., trends in the band structure of films as they become progressively thicker,[11] and possible band-structure effects in the quantum-size effect of thin metal films.[14]

II. FORMULATION

In this section we summarize our method as it applies to NFE metals, with particular application to the (001) surface of lithium in the bcc structure. We consider a film of N_3 atomic (001) planes, taking the origin of our coordinate system midway between the two surface planes and the coordinate z to be along the surface normal. Vectors perpendicular to the surface normal will be distinguished by an over-bar, e.g., $\bar{r} = (x, y)$ so that $\vec{r} = (\bar{r}, z)$. To make use of the symmetry under reflection in *bulk* (001) planes, we take N_3 odd, $N_3 = 2n_z + 1$, so that our film origin coincides with a z-reflection plane. Since reflection in this median plane is a symmetry operation for the film but does not effect $\bar{r}$ coordinates, we can discuss planar and z symmetry separately. (For an example of a case in which $\bar{r}$ and z symmetries are necessarily intertwined, see the treatment of an fcc (111) film in Ref. 11c). For the (unreconstructed) bcc (001 film of lattice constant a and N_3 odd, we denote the positions of the ions by $\vec{r}(\bar{l}, l_z) = (\bar{l} + \bar{x}(l_z), x_z(l_z))\, a$, where $\bar{l} = (l_x, l_y)$ and the l_α are integers with $|l_z| \leq n_z$. The planar origin is chosen at an ion in the median plane so that $\bar{x}(l_z) = (0, 0)$ for l_z even ("A planes") and $\bar{x}(l_z) = (\frac{1}{2}, \frac{1}{2})$ for l_z odd ("B planes").

The z coordinate of an ion is given by $x_z(l_z) = \frac{1}{2}[l_z + s(l_z)]$, where $s(l_z)$ is the cumulative fractional displacement due to relaxation.

In Fig. 1 we display the two-dimensional surface unit cell (SUC) of the diperiodic lattice $\bar{r}(\bar{l}) = \bar{l}a$ and the associated SBZ; the diperiodic reciprocal lattice vectors we denote by $\bar{G}_{\bar{m}} = (m_x, m_y)2\pi/a$, m's = integers. For the $\bar{r}$ variation we may expand the pseudo wave function of wave vector $\bar{k}$ in the SBZ in a set of 2DPW's of the form

$$\langle \bar{r} | \bar{k} + \bar{G} \rangle = (\bar{N}\mathcal{A}_0)^{-1/2} e^{i(\bar{k}+\bar{G})\cdot\bar{r}} , \tag{2.1}$$

where we invoke periodic boundary conditions in $\bar{r}$ with a total of $\bar{N}$ SUC's included and where $\mathcal{A}_0$ is the area of a SUC (here $\mathcal{A}_0 = a^2$). When $\bar{k}$ lies on a point or line of high symmetry, we construct symmetrized-2DPW's (S2DPW) transforming according to the required irreducible representations (irrep) of the group of $\bar{k}$; the Appendix summarizes the group theoretical notations and results we require here.

We deal with the remaining z variation of the wave functions in a plane-wave manner also. But now we have to treat both the approximately bulk-like behavior in the pseudopotential in the deep interior of the film and the strong deviations from bulk behavior in the selvage[15] region. We define a length L sufficiently large that for our purposes the electronic charge density is negligible at $z = \pm L$. The three-dimensional film unit cell, defined by the right parallelepiped whose cross section is the SUC and whose z extent is in principle $\pm\infty$, is thus assumed to be truncated at $z = \pm L$, and we assume that the z variation of the wave functions can be adequately expanded in the following truncated set of even and odd functions which vanish at $z = \pm L$:

$$\begin{aligned} \langle z | k_z^o \rangle &= L^{-1/2} \cos k_z^+ z, \quad k_z^+ = (2n-1)\pi/2L \\ &= L^{-1/2} \sin k_z^- z, \quad k_z^- = (2n)\pi/2L , \end{aligned} \tag{2.2}$$

where $n = 1, 2, 3, \ldots, n_L$. The number n_L of these functions required will depend, of course, on the size of L, which in turn depends on the number of ionic planes N_3 in the film and on the size of the assumed length of the outer selvage; as reported in AK, we found for the 13-layer Li (001) film that it was sufficient to take an outer-selvage of the extent of three unoccupied atomic planes at each surface ($2L = \frac{19}{2}a$), and $n_L = 30$.

The full basis functions are products of an even or odd function of z from Eq. (2.2) and an appropriate S2DPW:

$$\langle \bar{r}, z | j^o(\bar{k} + \bar{G}, k_z^o) \rangle = \langle \bar{r} | j(\bar{k} + \bar{G}) \rangle \times \langle z | k_z^o \rangle , \tag{2.3}$$

where the label j is a compound label standing for the full specification of the S2DPW. (See the Appendix.) Expansion of a crystal wave function of a given symmetry j^o at a given $\bar{k}$ in terms of the appropriate basis functions

$$| \psi(\bar{k}, j^o) \rangle = \sum_{\bar{G},\, k_z^o} | j^o(\bar{k} + \bar{G}, k_z^o) \rangle c(\bar{G}, k_z^o; \bar{k}, j^o) \tag{2.4}$$

leads to a matrix eigenvalue equation of the usual kind

$$\sum_{\alpha'} (H_{\alpha\alpha'} - E\delta_{\alpha\alpha'}) c(\alpha'; \bar{k}, j^o) = 0 \tag{2.5}$$

[where $\alpha = (\bar{G}, k_z^o)$] of dimension $n_L \times n_{\bar{G}}$, where $n_{\bar{G}}$ is the number of S2DPW's kept in the truncated basis set ($n_{\bar{G}}$ as large as 7 along the $\bar{\Delta}$, $\bar{Y}$, and $\bar{\Sigma}$ lines in the present work, corresponding to $|\bar{G}| \lesssim 4\pi/a$). Equation (2.5) may be solved by standard methods.[16] The Hamiltonian is of the usual form (Ry a.u., $\hbar = 2m = \frac{1}{2}e^2 = 1$)

$$H = -\nabla^2 + V_{ps} , \tag{2.6a}$$

where

$$V_{ps} = V_{loc} + V_{rep} , \tag{2.6b}$$

so that the kinetic energy matrix elements in Eq. (2.5) are diagonal:

$$(-\nabla^2)_{\alpha\alpha'} = [\, |\bar{k} + \bar{G}|^2 + (k_z^o)^2 \,] \delta_{\alpha\alpha'} .$$

The repulsive potential V_{rep} was chosen for our Li calculation as follows. We took a bulk-crystal pseudopotential to be a superposition of nonlocal, but energy-independent atomic pseudopotentials of the form

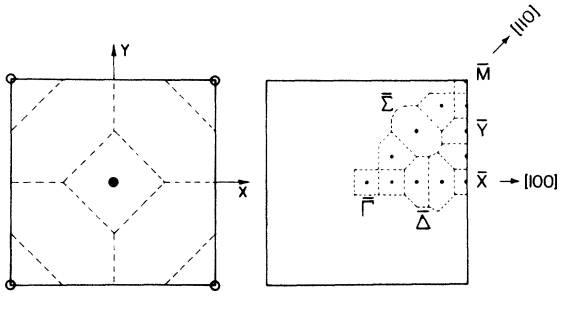

FIG. 1. Surface unit cell (SUC) and surface Brillouin zone (SBZ) for bcc (001). For the SUC, dashed lines depict projected edges of the conventional three-dimensional primitive unit cell; the origin is chosen with atoms of A planes (solid circles) in the center of the SUC and atoms of B planes (open circles) at the corners. (The x axis corresponds to a bulk [100] direction and y to [010].) For the SBZ, the points $\bar{\Gamma}$, $\bar{X}$, $\bar{M}$, and lines $\bar{\Delta}$, $\bar{\Sigma}$, $\bar{Y}$ of high symmetry are labeled according to the scheme in Ref. 2a. The sampling points in the irreducible $\frac{1}{8}$th part used in the present calculation are shown, with the boundaries of their proximity cells shown by dashed lines.

$$v_{ps}(\vec{r},\vec{r}\,') = v(\vec{r})\delta(\vec{r}-\vec{r}\,') + E_{rep}\phi_{1s}(\vec{r})\phi_{1s}(\vec{r}\,') , \tag{2.7}$$

where the atomic potential $v(\vec{r})$ and the $1s$ core wave functions $\phi_{1s}(\vec{r})$ were calculated with the Herman-Skillman program.[17] The parameter E_{rep} was adjusted so as to bring the bulk gap at the N point $(\frac{1}{2},\frac{1}{2},0)$ into approximate agreement with the first-principles results of Callaway[18] and Ham[19]; for the lattice constant $a = 3.449$ Å $= 6.518$ bohr which we adopted,[18] we chose $E_{rep} = 4.4884$ to give $\Delta_N E = E(N_1) - E(N_1\,') = 0.209$ Ry. In all our subsequent calculations, the film repulsive potential was

$$V_{rep}(\vec{r},\vec{r}\,') = \sum_{\bar{l},l_z} 4.4884\phi_{1s}(\vec{r}-\vec{r}(\bar{l},l_z)) \times\phi_{1s}(\vec{r}\,'-\vec{r}(\bar{l},l_z)) . \tag{2.8}$$

The initial thin-film potential was also chosen as a superposition of atomic pseudopotentials of the form (2.7). The local potential $v(r)$, however, required further adjustment to deal with the problem of $2s$ exchange. The $2s$ electrons in the $\rho^{1/3}$ exchange potential add a very long tail to the atomic potential; this appears, for example, as a pronounced shoulder on a graph of $-rv(r)$ vs $\log_{10} r$ extending from about $r = 1.0$ to 2.3 Å before $rv(r)$ resumes its regular decay. The result of the $2s$-exchange tail is to yield a narrow but large negative peak in the Fourier transform

$$v(\vec{K}) = \Omega_a^{-1}\int d^3r\, v(\vec{r})e^{-i\vec{K}\cdot\vec{r}}, \quad \Omega_a = \tfrac{1}{2}a^3, \tag{2.9}$$

which does not effect the bulk band structure except for an over-all shift [given by $v(K=0) = -5.2$ Ry.] because the bulk reciprocal-lattice vectors lie beyond the peak. For thin films, however, the smaller k_z's of Eq. (2.2) will sample this peak and bias the initial film eigenvalues toward unphysically large negative energies relative to the vacuum level. With the exchange peak in $v(K)$, the Fermi level below the vacuum level yields a work function an order of magnitude too large, an error which the relatively small surface dipole layer cannot correct. Since the error lies in superposing atomic $\rho^{1/3}$ potentials, which are not additive because of the overlap of $2s$ contributions from near-neighbor atoms, and since the self-consistent calculation for the film will treat the extended valence charge distribution properly, we obtained a starting potential by adjusting the amount of atomic $2s$-exchange contribution to $v(r)$ as follows. First, we calculated an atomic potential $v_{\rm I}(r)$ from the Herman-Skillman charge density, using both the φ_{1s} and ϕ_{2s} wave functions to calculate the Coulomb contribution but only the ϕ_{1s} functions to calculate the $\rho^{1/3}$ exchange contribution; this gave $v_{\rm I}(K=0) = -0.7334$ Ry. Second, we calculated $v_{\rm II}(r)$ by deleting $2s$ contributions to the $\rho^{1/3}$ exchange potential entirely from the Herman-Skillman program; this gave $v_{\rm II}(K=0) = -1.0941$ Ry. For the calculation reported in AK, we estimated that a weighted average $\bar{v}$ of $v_{\rm I}$ and $v_{\rm II}$ such that $\bar{v}(K=0) = -0.877$ Ry would yield a fairly good approximation to the experimental value 0.183 Ry reported for the work function.[20] The actual value found in the AK film potential was $-E_F = 0.257$ Ry. Although there is considerable uncertainty in the experimental situation regarding the work function of lithium,[8c] we began our series leading to self-consistency with a new weighted average adjusted upward such that $\bar{v}(K=0) = -0.800$ Ry. (Interestingly enough, it developed that our self-consistent potential has an interior average very close to the initial potential in AK.)

With a given local part of the film potential $V_{\rm loc}$ and the repulsive potential $V_{\rm rep}$ of Eq. (2.8), we calculate the crystal states having energies near or below the vacuum level at a set of sample $\bar{k}$ points in the SBZ; the 12 independent sample points we used are shown in Fig. 1, with each surrounded by a proximity cell whose boundaries are shown by dashed lines and whose relative area is proportional to the weight given the contained sample point. The valence charge density[21] is then obtained, in units of $-e$, as

$$\rho(\bar{r},z) = 2\sum_{\bar{k}}^{\rm IE} w(\bar{k}) \sum_{*\bar{k}} \sum_{j\sigma\beta}^{\rm occ} |\psi(\bar{r},z;\bar{k},j^\sigma,\beta)|^2 , \tag{2.10a}$$

where the occupied levels are determined by a calculation of the Fermi level E_F such that

$$N_3 Z_{\rm val} = 2\sum_{\bar{k}}^{\rm IE} w(\bar{k}) \sum_{*\bar{k}} \sum_{j\sigma\beta} \theta[E_F - E(\bar{k},j^\sigma\beta)] , \tag{2.10b}$$

and for our 13-layer Li (001) film $N_3 Z_{\rm val} = 13$. In Eqs. (2.10) the first sum is over the independent sample $\bar{k}$ points in the $\frac{1}{8}$th irreducible element (IE) of the SBZ, with $w(\bar{k})$ the weight of the sample point equal to the relative area of its proximity cell in Fig. 1. The second sum is over the star of $\bar{k}$ and serves to symmetrize the result so that $\rho(\bar{r},z)$ has the full two-dimensional symmetry of the film (here $\bar{\Gamma}_1$ of C_{4v}). The last sum is over the occupied levels of symmetry j^σ, with β the band index if more than one $(\bar{k}\,j^\sigma)$ level is occupied. (Several levels were close enough to each other and to the Fermi level that they were entered in the last sum with a fractional, rather than unit, occupation number.) The charge density, as well

as the local part of the film potential, may be resolved into Fourier components as

$$\rho(\vec{r},z)=\sum\rho_{\vec{G}}(z)e^{i\vec{G}\cdot\vec{r}}$$

$$=\sum_{\vec{G}_p}\rho_{\vec{G}}(z)F_{\vec{G}_p}(\vec{r}) \qquad (2.11)$$

and

$$\rho_{\vec{G}}(z)=\sum_q\rho_{\vec{G}q}\cos qz\ , \qquad (2.12)$$

where

$$F_{\vec{G}_p}(\vec{r})=\sum_{*\vec{G}_p}e^{i\vec{G}\cdot\vec{r}} \qquad (2.13)$$

and $q=n\pi/2L$, $n=0,1,2,\ldots,2n_L$.[22] In Eq. (2.11) $\vec{G}_p$ is a prototype $\vec{G}$ vector in a particular star of two-dimensional reciprocal wave vectors; the functions $F_{\vec{G}}(\vec{r})$ are thus (un-normalized) basis functions transforming as the $\bar{\Gamma}_1$ irrep. (the first 12 such functions are tabulated in the Appendix, since they arise in multiplying out the S2DPW's used in this calculation). We calculated $\rho_{\vec{G}}(z)$ by writing a computer program that accumulates the various contributions to each $\vec{G}$ component obtained by multiplying out the 2DPW's from each product of S2DPW's occurring in

$$\left|\,|\psi(\vec{k},j^\sigma,\beta)\rangle=\sum_{\vec{G},k_z^Q}|j^\sigma(\vec{k}+\vec{G},k_z^\sigma)\rangle c(\vec{G},k_z;\ \vec{k},j^\sigma,\beta)\right|^2;$$

this was done on a uniform mesh along z, which in this work was 20 intervals between adjacent ionic planes.

With the charge density in hand, we may then calculate the local part of the crystal potential $V_{\rm loc}^{\rm out}$ resulting from an input local potential $V_{\rm loc}^{\rm in}$ as a sum of three parts

$$V_{\rm loc}^{\rm out}=V^{\rm core}+V^{\rm Coul.}+V^{\rm xc}\ . \qquad (2.14)$$

Here the individual components are, respectively, the fixed potential of the neutral 1s-ion core, the Coulomb potential arising from the Hartree potential of the valence electrons and the array of compensating protons, and the valence exchange-correlation potential. $V^{\rm core}$ is the superposition of neutral ion-core potentials calculated with the ϕ_{1s} wave functions from the Herman-Skillman program and the compensating pair of protons in each core; if we define the bulk spatial average of a local potential as being the spatial average over two interplanar intervals in the center of the film,

$$\langle V\rangle_{\rm bulk}\equiv\frac{1}{a}\int_0^a dz\,V_{\vec{0}}(z), \qquad (2.15)$$

then we have $\langle V^{\rm core}\rangle_{\rm bulk}=v^{\rm core}(K=0)=-0.270$ Ry.

(Although we keep $V^{\rm core}$ fixed in the present calculation, we consider it to be a part of the "output" potential to facilitate comparison with the input potential.) The Fourier coefficients of the Coulomb potential are given by

$$V_{\vec{G}q}^{\rm Coul.}=8\pi(\vec{G}^2+q^2)^{-1}[\,\rho_{\vec{G}q}-\mathcal{S}(\vec{G},q)/\mathcal{A}_0L], \qquad (2.16)$$

where $\rho_{\vec{G}q}$ is obtained by numerically inverting (2.12), the symmetrized film structure factor is given by

$$\mathcal{S}(\vec{G},q)=1+2\sum_{m=1}^{n_{3A}}\cos\frac{2mqa}{2}$$

$$+2\cos(\tfrac{1}{2}aG_x)\cos(\tfrac{1}{2}aG_y)$$

$$\times\sum_{m=1}^{n_{3B}}\cos[\tfrac{1}{2}(2m-1)(qa)], \qquad (2.17)$$

$2n_{3A}$ is the number of A planes (excluding the central plane) and $2n_{3B}$ is the number of B planes in the film. The $(\vec{0},0)$ component $V_{\vec{0},0}^{\rm Coul.}$ is found by taking one-half[22] of the $q\to 0$ limit of Eq. (2.16).[23]

The final contribution to $V_{\rm loc}^{\rm out}$ is the exchange-correlation potential $V^{\rm xc}$. As intimated in Sec. I, we treat this in a local approximation, as did AH. We differ on the particular local approximation used. AH chose the $X\alpha$ potential in the form $V^{\rm xc}(r)=F[\,\rho(r)]^{1/3}$, although they did not report their choice for the factor F. We chose to use the Wigner interpolation form as used by Lang and Kohn[8]

$$V^{\rm xc}=\frac{\partial(\rho\epsilon_{\rm xc})}{\partial\rho}\ , \qquad (2.18)$$

where

$$\epsilon_{\rm xc}=-0.916/r_s(\rho)-0.88/[r_s(\rho)+7.79], \qquad (2.19)$$

so that

$$V^{\rm xc}=-\tfrac{4}{3}A\rho^{1/3}-\frac{\frac{4}{3}B\rho^{1/3}}{1+C\rho^{1/3}}+\frac{\frac{1}{3}BC\rho^{2/3}}{1+C\rho^{1/3\ 2}}\ , \qquad (2.20)$$

where $A=0.916(\frac{4}{3}\pi)^{1/3}$, $B=0.88(\frac{4}{3}\pi)^{1/3}$, and $C=7.79(\frac{4}{3}\pi)^{1/3}$. The $\vec{G}=0$ component of $\rho(\vec{r},z)$ is the dominant contribution in a NFE metal. We write

$$\rho(\vec{r},z)=\rho_{\vec{0}}(z)[1+\bar{\rho}(\vec{r},z)], \qquad (2.21)$$

where $\bar{\rho}(\vec{r},z)\equiv\sum{}'\bar{\rho}_{\vec{G}}(z)\,e^{i\vec{G}\cdot\vec{r}}$, $\bar{\rho}_{\vec{G}}(z)\equiv\rho_{\vec{G}}/\rho_{\vec{0}}$, and the prime on the sum indicates that the $\vec{G}=0$ term is omitted. The function $\bar{\rho}(\vec{r},z)$ is a small quantity, and we evaluated the $\vec{G}$ components of $V^{\rm xc}$ by expanding the various terms of Eq. (2.20) in Taylor series in $\bar{\rho}(\vec{r},z)$ to third order and collecting terms. For example,

$$\rho(r)^{1/3} = \rho_{\bar{0}}(z)^{1/3}\left[1+\frac{1}{3}\sum_{\bar{G}}{}'\bar{\rho}_{\bar{G}}(z)\,e^{i\bar{G}\cdot\bar{r}} - \frac{1}{9}\left(\sum_{\bar{G}}{}'\bar{\rho}_{\bar{G}}(z)\,e^{i\bar{G}\cdot\bar{r}}\right)^2+\cdots\right]$$

$$= \rho_{\bar{0}}(z)^{1/3}\left(\left[1-\tfrac{1}{9}\bar{\bar{\rho}}_{\bar{0}}(z)\right]+\sum_{\bar{G}}{}'\left[\tfrac{1}{3}\bar{\rho}_{\bar{G}}(z) - \tfrac{1}{9}\bar{\bar{\rho}}_{\bar{G}}(z)\right]e^{i\bar{G}\cdot\bar{r}}\right), \tag{2.22}$$

where

$$\bar{\bar{\rho}}_{\bar{G}} \equiv \sum_{\bar{G}'}{}'\bar{\rho}_{\bar{G}'}(z)\bar{\rho}_{\bar{G}-\bar{G}'}(z)$$

and the prime on this sum means neither $\bar{G}'$ nor $\bar{G}-\bar{G}'$ may be zero. These expansions yield $V^{xc}_{\bar{G}}(z)$ in an adequate approximation since the maximum $\bar{\rho}_{\bar{G}}(z)$ is 0.04, and a numerical Fourier inversion of Eq. (2.12) with $V^{xc}_{\bar{G}}(z)$ replacing $\rho_{\bar{G}}(z)$ gives us the film Fourier transform $V^{xc}_{\bar{G},q}$ required in construction of the Hamiltonian matrix.

With V^{out}_{loc} determined, we compare it with the V^{in}_{loc} which generated it, in order to assess the degree of self-consistency of the input potential and to seek guidance on how to improve the input potential so as to more closely approach self-consistency. The improvement of the input potential from the information contained in its output potential is not a trivial matter, and we devote the remainder of this section to this subject. In bulk-band-structure calculations that go beyond use of linear response and a dielectric function to achieve self-consistency, the standard procedure is iteration or some simple modification of iteration—usually a linear mixture of input and output potentials of one stage ("old") to give the input potential for the next ("new")

$$V^{(in)}(\text{new}) = (1-\alpha)V^{(out)}(\text{old}) + \alpha V^{(in)}(\text{old}), \quad 0 \leq \alpha < 1. \tag{2.23}$$

We found, as did Lang and Kohn[8] and AH, that iteration in surface calculations is a highly unstable procedure as far as the $\bar{G}=0$ components of potential are concerned; as experienced by AH, we found that the $\bar{G}\neq 0$ components converge rapidly with iteration. AH did find a modified iteration of the form (2.23) for $\bar{G}=0$ would converge in their method, if α were taken as large as 0.9 in the first iterations and going down to as low as 0.6 in the last few. We believe that their success in using this kind of iteration depends in large part on forcing the inner selvage region to terminate absolutely at the matching plane between the second and third or the third and fourth atomic planes. It may be possible that some of the success of iteration is due to the complete neglect of evanescent waves on the bulk side of the matching plane, justified in AH on the grounds that the bulk potential obtains immediately on the bulk side of the matching plane and, implicitly, on the grounds that no occupied surface states should appear in monovalent NFE metals such as sodium.

As did Lang and Kohn[8] we did not find iteration in any simple form to be a usable procedure, and we had to discover more artful means of approaching the self-consistent $\bar{G}=0$ component of the potential. Before taking up a discussion of our procedure we should point out two interrelated sources of the instability under iteration. First, very small changes in the selvage charge density give rise to large changes in the (extended) surface dipole layer, causing large changes in the interior bulk potential relative to the vacuum. In the outer selvage where ρ is very small, the Coulomb potential is negligible whereas the exchange potential is still quite large (the cube root is a great enhancer). The second source of instability is the "antiscreening" effect of the exchange potential; the increase of charge density in the outer selvage lowers $V^{xc}_{\bar{0}}$ there, tending to draw in more charge rather than expelling charge as the Hartree term does.

In light of our experience with the calculation reported here, we would divide the approach to self-consistency into two stages. The initial stage is concerned with getting the potential roughly correct in all three regions—bulk, inner selvage, and and outer selvage. The procedure we actually used in this initial calculation was a rather *ad hoc* combination of averaging $V_{\bar{0}}(z)$ functions and splicing together pieces of such functions obtained from different domains of z; we do not especially recommend it and we shall not describe it further. A procedure we do recommend is that adopted in Ref. 11 whereby the bulk potential (already as self-consistent as possible) is continued up to the nominal surface plane; this bulk potential is modulated in the inner selvage by multiplying by the factor $[v_{eff}(+\infty)-v_{eff}(z)]/[v_{eff}(+\infty)-v_{eff}(-\infty)]$ drawn from the calculation of Lang and Kohn,[8b] and the potential in the outer selvage is obtained by matching the jellium potential smoothly with the modulated bulk potential in the inner selvage. (This, of course, means that exchange and correlation should be treated in the same way as Lang and Kohn.) This procedure has the advantage over the initial potential in AH that the Friedel oscillations are to some extent synthesized into the initial potential, and if necessary the jellium edge of the Lang-Kohn potential can be shifted relative to the nominal surface plane so as to include the best initial estimate of the dipole layer, as was done in

AH. The second stage of our procedure bears a slight resemblance to the procedure of Lang and Kohn, except that we focus on the potential rather than the charge density. Starting with a reasonably approximate potential $V_0^{(1)}$ and its output potential $V_0^{(2)}$; we form a new input potential $V_0^{(2)} = (1-\alpha_2)V_0^{(1)} + \alpha_2 V_0^{(1)}$ and calculate its output $V_0^{(2)}$; α_2 is chosen according to the degre of agreement between $V_0^{(1)}$ and $V_0^{(1)}$, with a typical value of 0.85 near the end of the series. Next, another input $V_0^{(3)} = (1-\alpha_3)V_0^{(2)} + \alpha_3 V_0^{(2)}$ is formed with α_3 chosen so as to give an error $[V_0^{(3)}(z=0) - V_0^{(3)}(z=0)]$ approximately equal and opposite to $[V_0^{(2)}(0) - V_0^{(2)}(0)]$; a typical value corresponding to the above α_2 is $\alpha_3 = 0.97$. Finally, the improved approximate potential is calculated as $V_0^{(4)} = (1-\alpha_4)V_0^{(2)} + \alpha_4 V_0^{(3)}$, with α_4 chosen so as to make $V_0^{(4)}(z)$ as level as possible in the bulk region; for example by choosing α_4 such that

$$(1-\alpha_4)\left\langle \frac{\partial V_0^{(2)}}{\partial z}\right\rangle_{\text{bulk}} + \alpha_4 \left\langle \frac{\partial V_0^{(3)}}{\partial z}\right\rangle_{\text{bulk}} = 0,$$

where $\langle \cdots \rangle_{\text{bulk}}$ is defined by Eq. (2.15). In Sec. III we present and discuss the results of our calculation for the unrelaxed 13-layer Li (001) film.

III. RESULTS AND DISCUSSION

We begin the presentation of results with the potential, since the agreement between input and output potential provides the criterion for judging self-consistency. Figure 2 displays the first six Fourier coefficients $V_{\bar{G}}(z)$ of the final total local input[24] potential which is self-consistent to within 0.001 Ry over all values of z. The maximum error of +0.00105 Ry (output higher than input) between input and output values of $V_{\bar{0}}(z)$ for this potential occurs at the nominal jellium edge $z/\frac{1}{2}a = 6.5$, and the error has fallen to +0.0006 at $z/\frac{1}{2}a = 7.0$. A region of about +0.0008-Ry error extends from $z/\frac{1}{2}a \approx 6.0$ (outer plane) to 5.0 (first subsurface plane). Over the rest of the film the error is less than 0.0005 Ry in magnitude, and in the region $|z/\frac{1}{2}a| < 1.5$, the error oscillates in sign with amplitude about 0.0001 Ry; the bulk averages of the input and output are $\langle V_0^{(\text{in})}\rangle_{\text{bulk}} = -0.872005$ Ry and $\langle V_0^{(\text{out})}\rangle_{\text{bulk}} = -0.872055$ Ry.

The rapid achievement of self-consistency in the $\bar{G} \neq 0$ components is illustrated by the fact that on the scale of Fig. 2 these components of the self-consistent potential could not be distinguished from those of either of the two initial superpositions of atomic potentials mentioned in Sec. II; consequently, we need no further discussion of the $\bar{G} \neq 0$ components of potential. In contrast, although the $\bar{G} = 0$ components of the self-consistent potential [labeled (00)F] and the superposition of atomic potentials used in AK [labeled (00)I] agree closely in the bulk region, they differ substantially in the selvage region. Their bulk averages in the middle of the film are $\langle V_{\bar{0}I}\rangle_{\text{bulk}} = -0.8770$ Ry and $\langle V_{\bar{0}F}\rangle_{\text{bulk}} = -0.8720$ Ry. On the other hand, over

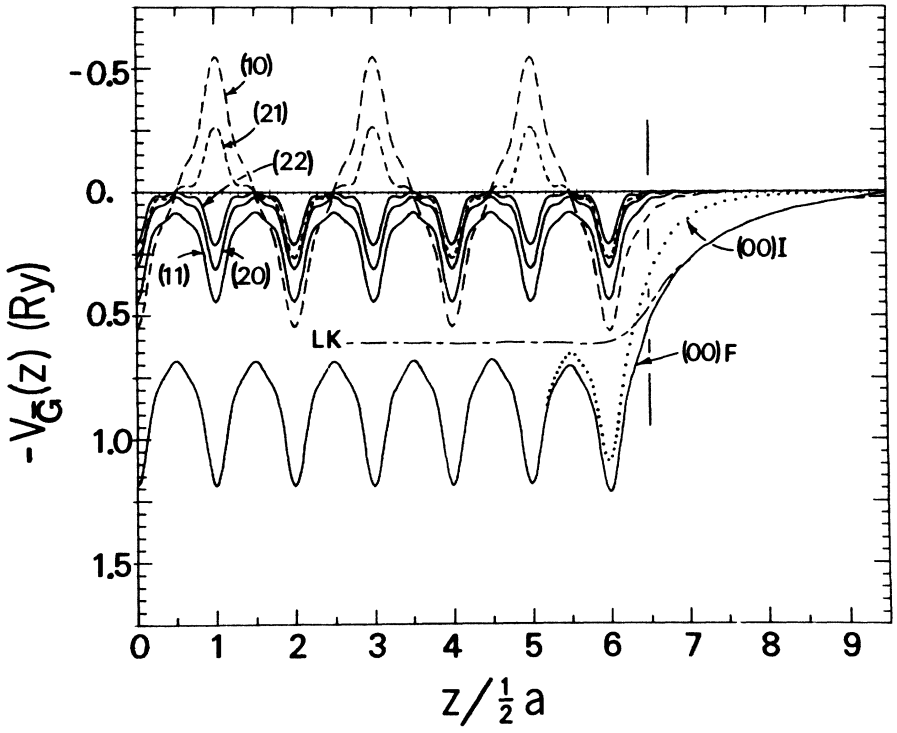

FIG. 2. Planar Fourier components of the local part of the pseudopotential, $V_{\bar{G}}(z)$, for $\bar{G}$ up to $\bar{G} = (2,2)2\pi/a$. The nominal jellium edge at $z/\frac{1}{2}a = 6.5$ is marked by the vertical broken line. For $\bar{G} = 0$, (00)I denotes the initial potential and (00)F denotes the final, self-consistent (input) potential. LK labels the Lang-Kohn v_{eff} for $r_s = 3.209$, shifted to zero value at the vacuum level.

most of the outer selvage region the self-consistent $V_{\bar{0}}(z)$ is seen to agree closely with the jellium result LK (for which $\langle V_{LK}\rangle_{bulk} = -0.609$ Ry) obtained by linear interpolation for $r_s = 3.209$ from the Lang-Kohn tables.[8b] The slight disagreement near $z/\frac{1}{2}a = 9.5$ is to be expected because our choice of basis functions forces the charge density, hence $V^{Coul.} + V^{xc}$, to vanish there. Near the jellium edge, the lattice aspect of the crystalline potential causes it to deviate noticeably from LK. In the innerselvage region, the self-consistent potential $V_{\bar{0}}(z)$ show effects of Friedel oscillation to a degree greater than the jellium result. The LK curve at $z/\frac{1}{2}a = 5.7$ dips to 0.006 Ry below its bulk value. On the other hand, relative to the corresponding points in the center of the film [for which $V_{\bar{0}}(z) = V_{\bar{0}}(z \pm \frac{1}{2}a)$ to within ±0.0015 Ry for $-2.5 \leq z/\frac{1}{2}a \leq 2.5$], $V_{\bar{0}F}(z)$ is displaced downward by about 0.029 Ry at the first ionic plane ($z/\frac{1}{2}a = 6.0$), downward about 0.020 Ry midway between the first and second plane, upward about 0.004 Ry at the second plane, and upward about 0.006 Ry between the second and third planes. At the third plane and midway between the third and fourth planes the potential is well within the ±0.0015 Ry variation but then drops downward about 0.003 Ry at the fourth plane ($z/\frac{1}{2}a = 3$).

The three local contributions to the self-consistent potential $V_{\bar{0}}(z)$ have the following bulk averages: $\langle V_{\bar{0}}^{core}\rangle_{bulk} = -0.2700$ Ry, $\langle V_{\bar{0}}^{Coul.}\rangle_{bulk} = -0.1340$ Ry, and $\langle V_{\bar{0}}^{xc}\rangle_{bulk} = -0.4681$ Ry. $\langle V_{\bar{0}}^{Coul.}\rangle_{bulk}$ is to be compared with the dipole-layer potential found in jellium, which is $-\Delta\phi = -0.143$ Ry based on linear interpolation for $r_s = 3.209$ from the improved values in Ref. 8c. The nonlocal repulsive potential is not easily represented in a figure such as Fig. 2. Its effect can be seen by the fact that the lowest energy level in the self-consistent 13-layer film is $E_1(\bar{\Gamma}_1^+) = -0.5004$ Ry; the plane-wave diagonal matrix elements of the repulsive atomic potential of Eq. (2.7), $\langle \vec{K}|v_{rep}|\vec{K}\rangle$, vary slowly from +0.3749 Ry at $K = 0$ to +0.3034 Ry at $K_F \approx (0.6)2\pi/a$. Compare $E_1(\bar{\Gamma}_1^+)$ with $\langle V_{\bar{0}}^{core}\rangle_{bulk} + \langle V_{\bar{0}}^{Coul.}\rangle_{bulk} + \langle V_{\bar{0}}^{xc}\rangle_{bulk} + \langle 0|v_{rep}|0\rangle = -0.4972$ Ry. The Fermi level relative to the vacuum level is −0.2726 Ry for a work function of 3.71 eV. This value is to be compared with the first-order pseudopotential corrected value 3.30 eV by Lang and Kohn[8c] and the two "standard" experimental values for polycrystalline samples, 2.32 and 3.1 eV, cited by them. At least part of the larger value of our result probably arises from our choice of the E_{rep} parameter; we will return to a discussion of this point toward the end of this section.

We next take up the charge density. In the self-consistent potential for the 13-layer Li (001) film, the 12 independent sample points of Fig. 1 yield 78 independent occupied levels (seven of which are within −0.005 to +0.002 of E_F and are treated with fractional occupation numbers). Figure 3 displays the resulting charge density $\rho(\bar{r}, z)$ from the middle of the film outward to $z = L$ for six typical values of the planar coordinate $\bar{r}$. Comparison of this $\rho(\bar{r}, z)$ with that in AK reveals marked differences. The sharply rising barrier presented by the non-self-consistent potential $V_{\bar{0}1}$ severely distorts the charge density in AK, raising the charge density to values significantly greater than the proper bulk values over most of the volume of the film, mainly as a result of forcing charge density from both inner and outer selvage regions into the bulk region. In contrast, the self-consistent potential produces a charge density which displays a large Friedel peak between the first and second surface plane over much of the SUC; the Friedel peak reaches its maximum value of about 2.55 electrons per a^3 immediately behind the surface atom.

In Fig. 4 we display the $\bar{G} = 0$ component of $\rho(\bar{r}, z)$, which is the planar average, and for comparison the jellium result interpolated from the Lang-Kohn tables.[8b] In the bulk region, $\rho_{\bar{0}}(z)$ oscillates about the bulk average of 2.0 electrons per a^3 with an amplitude of about 0.09 electrons per a^3. The major Friedel peak appearing between the first and second ionic planes rises to a value

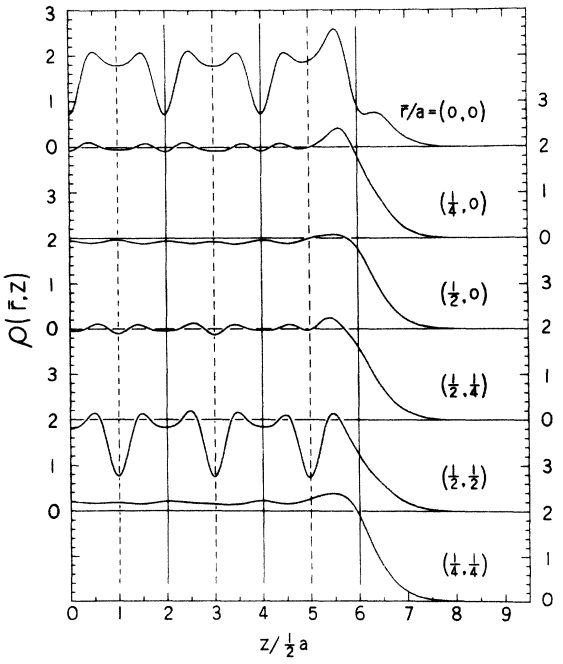

FIG. 3. Pseudocharge density $\rho(\bar{r}, z)$, in units of $-e$ per a^3, for selected values of $\bar{r}$. Locations of A planes are denoted by vertical solid lines, B planes by dashed lines.

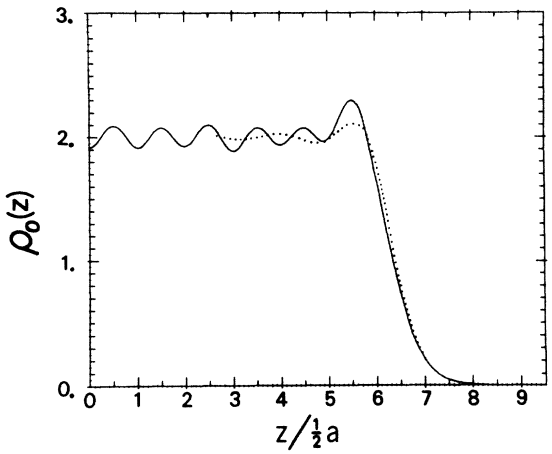

FIG. 4. Planar-average ($\bar{G}=0$ component) pseudocharge density $\rho_0(z)$, in units of $-e$ per a^3. The Lang-Kohn result for $r_s=3.209$ is shown as a dotted line.

of 2.300, which is to be compared with 2.108 for jellium. Thus we find an excess in the Friedel peak of 0.192 above the jellium peak, so that in contrast with the result for sodium in AH the crystal Friedel peak is not simply the superposition of the jellium peak of 0.108 on the bulk-crystal interplanar value of 2.09. It is seen that the wavelength of the Friedel oscillations is not commensurate with the interplanar spacing. This lack of registry appears to give rise to significant structure in $\rho_{\bar{0}}(z)$ at least as deep as the fourth atomic plane, which is marked by a pronounced minimum where a jellium minimum closely coincides with a bulk-crystal minimum.

The redistribution of charge in the neighborhood of the surface may be better appreciated by reference to Fig. 5 which shows charge-density contours over the first quadrant of the SUC from the jellium edge at $z/a=3.25$ to $z/a=2.40$ just inside the second ionic plane. The upper left octant contains the charge-density contours at the indicated value of z/a, while the lower right octant gives the contours for a corresponding bulk-like plane between $z/a=\pm 0.5$. The dashed diagonal line separating the two octants is a reflection plane $[(1\,\bar{1}\,0)]$ of symmetry of the film, and the heavy diagonal line marks the intersection of a $\{111\}$ face of the bulk Wigner-Seitz cell with the contour plane. We see that the surface "smoothing" redistribution of charge, invoked in 1941 by Smoluchowski[25] to help explain the dependence of the work function on the density of packing of the exposed face, causes the charge density to differ from that of the bulk not only in magnitude but by pattern as well.

Figure 6 displays the two-dimensional band

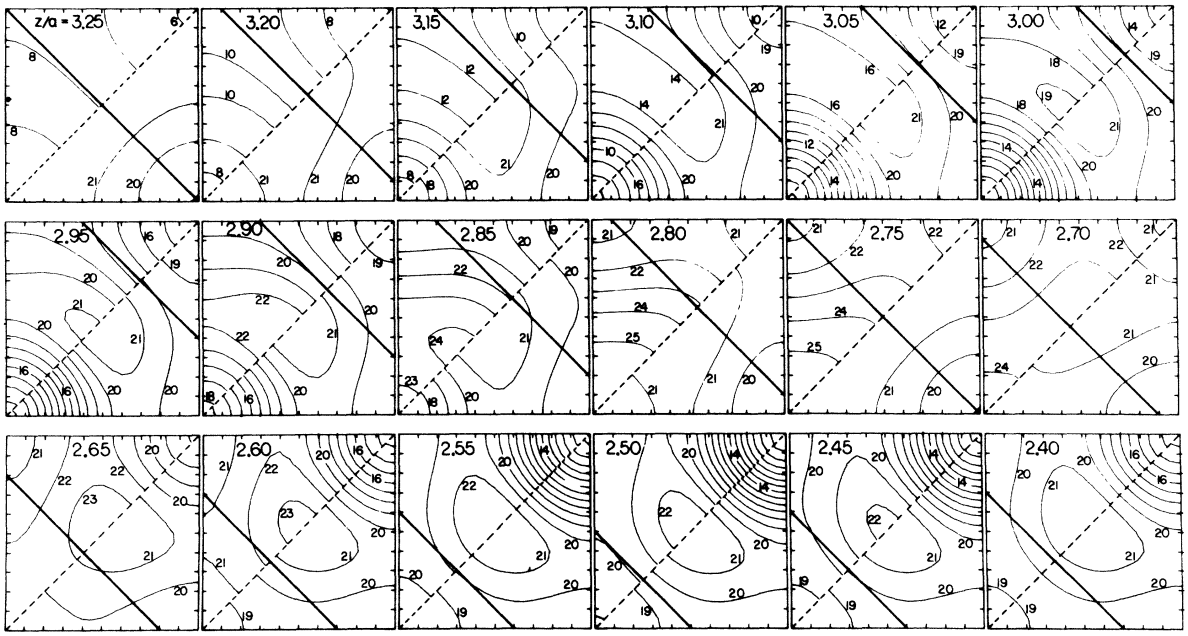

FIG. 5. Contour plots of pseudocharge density $\rho(\bar{r}, z)$ from the jellium edge at $z/a=3.25$ to $z/a=2.40$, just inside the first subsurface plane. The contour lines are at equal intervals of $-e/10$ per a^3. Each frame represents the first quadrant of the SUC (Fig. 1), with the upper octant (above the diagonal dashed line) showing the contours at the displayed value of z/a and, for reference, the lower octant showing the "bulk" contours drawn from the center of the film ($|z/a| \leq 0.25$). The heavy diagonal line passing from upper-left to lower-right side marks the intersection of the $\{111\}$ faces of the Wigner-Seitz cells with the various contour planes.

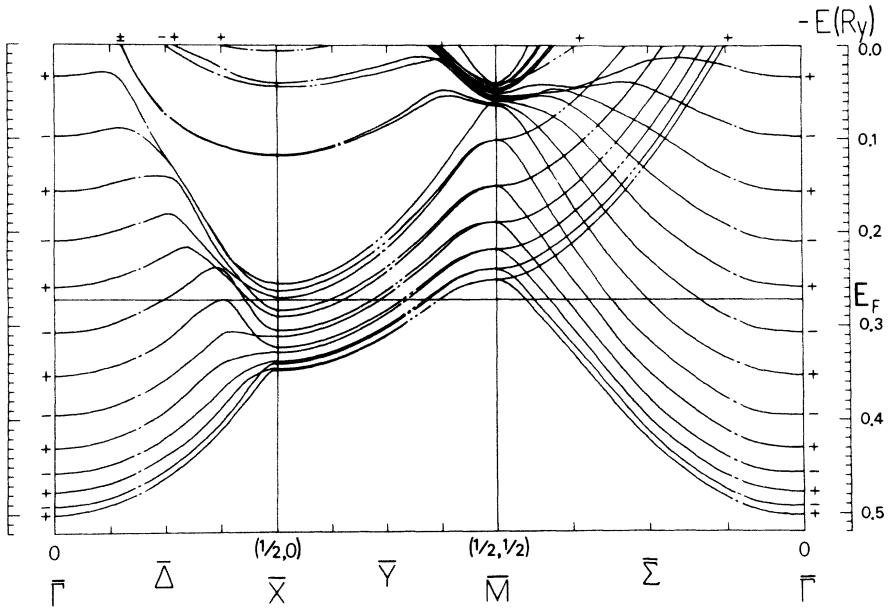

FIG. 6. Band structure of the self-consistent thirteen-layer Li (001) film. For the horizontal axis, the wave vector is in units of $2\pi/a$. The z symmetry of the states is labeled by the ± signs around the border. The planar symmetry along the lines $\bar{\Delta}$, $\bar{Y}$, and $\bar{\Sigma}$ is coded by the number of dots in the breaks in the lines (e.g., along $\bar{Y}$ two dots denote $\bar{Y}_2$), except for the uppermost region around $\bar{M}$ where the density of bands prevents labeling. All the $\bar{\Gamma}$ states are $\bar{\Gamma}_1$. The $\bar{X}$ states can be determined by the compatibility relations $\bar{X}_1 \rightarrow \bar{\Delta}_1$, $\bar{Y}_1$ and $\bar{X}_3 \rightarrow \bar{\Delta}_1$, $\bar{Y}_2$. The lowest six $\bar{M}$ levels are doubly degenerate $\bar{M}_5^+$ or $\bar{M}_5^-$, and above these are $\bar{M}_1^+$, $\bar{M}_1^-$, $\bar{M}_4^+$, $\bar{M}_1^+$, $\bar{M}_4^-$, $\bar{M}_1^-$, $\bar{M}_4^+$, $\bar{M}_1^+$, $\bar{M}_4^-$, $\bar{M}_1^-$, $\bar{M}_4^+$, and $\bar{M}_5^+$.

structure (up to vacuum level) which follows from the self-consistent potential. As in AK, the two lowest $\mathbf{X}$ levels, $\mathbf{X}_1^+$ and $\mathbf{X}_3^+$, correspond approximately to the lowest bulk levels at $(\pm\frac{1}{2}, 0, 0)$ in the infinite crystal. The levels in the densely populated region above these correspond roughly to increasing k_z in the infinite crystal. In the bulk, this quasicontinuum at $\mathbf{X}$ would extend up a level degenerate with the lowest $\bar{M}_5^+$ level, which in turn corresponds to the bulk N point $(\frac{1}{2}, \frac{1}{2}, 0)$. However, in the present case there is some question whether the $\mathbf{X}_3^+$ and $\mathbf{X}_3^-$ states at the very top of this quasicontinuum are bulk or surface states; we will return to this question below. Above this band there is a gap of 0.212 Ry to an $\mathbf{X}_3^-$ level corresponding to the $(\frac{1}{2}, 0, \frac{1}{2})$ gap of 0.209 Ry for the bulk crystal. Within the gap are two surface states $\mathbf{X}_1^\pm$ which are nearly degenerate. (We will return to the discussion of the surface states below after completing our discussion of the bulklike aspects of Fig. 6.) The lowest $\bar{\Sigma}_2^+$ branch leaving the lowest $\bar{M}_5^+$ level corresponds to the lowest-bulk-energy band running directly from $(-\frac{1}{2}, \frac{1}{2}, 0)$ to $(-1, 0, 0)$; at $\bar{M}_5^+$, it becomes exactly degenerate with the lowest $\bar{\Sigma}_1^+$ branch which corresponds to the lowest-bulk-energy band running directly from $(0, 0, 0)$ to $(\frac{1}{2}, \frac{1}{2}, 0)$. The branches above these also correspond roughly to increasing k_z in the bulk crystal, up to the dense accumulation at and near $\bar{M}$ at about -0.05 Ry which corresponds to the onset of both bulk N_1 states and the doubly degenerate bulk P_4 states.[19]

A comparison of Fig. 6 with the 2D band structure reported in AK reveals two principal differences in the bulklike bands. First, as mentioned above in connection with the charge density, the sharply rising surface barrier of the initial potential unduly confines the electrons in the z direction. Thus, although the lower edge of the band structure in Fig. 6 and in AK agree quite well (i.e., effective $k_z \simeq 0$), for given $\bar{k}$ the higher bulklike bands (effective $k_z > 0$) lie significantly higher in AK than in Fig. 6. The result is that in AK E_F lies significantly higher (relative to the bulk-band structure as given by the lowest $\bar{\Gamma}_1^+$ and $\bar{M}_5^+$) than does E_F in Fig. 6. For both band structures the band width of the lowest $\bar{\Sigma}_1^+$ is $E_1(\bar{M}_5^+) - E_1(\bar{\Gamma}_1^+) = 0.249$ Ry, but whereas Fig. 6 has 92% of this bandwidth occupied (in fairly close agreement with Ham[19] and Callaway[18]) AK has 99% of the bandwidth occupied. The second principal difference between Fig. 6 and AK is that the self-consistent potential gives rise to substantially greater splitting between $\mathbf{X}_1^\sigma$ and $\mathbf{X}_3^\sigma$ bulklike levels of the same parity σ. This is essentially a size effect, inasmuch as in the infinite crystal the $\mathbf{X}_1^\sigma$

and $\bar{X}_3^{\sigma}$ levels coalesce into degenerate pairs; these irreps differ simply by a translation from cube center (origin of SUC) to cube corner (corner of SUC), but in the infinite bcc crystal, cube centers and corners are indistinguishable.

Returning now to the surface states, we note that in the passage to self-consistency from the initial potential in AK the $\bar{X}_3$ surface states of AK have been depressed to the lower edge of the $\bar{X}$ gap, and $\bar{X}_1$ surface states have descended out of the bulk band above and down into the $\bar{X}$ gap to a level of about -0.117 Ry [actually, -0.1176 for $(\bar{X}_1^+)_4$ and -0.1166 Ry for $(\bar{X}_1^-)_4$]. To illustrate the development of this result, we have calculated the states at $\bar{X}$ in a linear mixture of the potential of AK and the self-consistent potential such that

$$V_{\bar{0}\alpha}(z) = (1-\alpha)V_{\bar{0}I}(z) + \alpha V_{\bar{0}F}(z) \,. \tag{3.1}$$

Figure 7 displays the evolution of the $\bar{X}$ states as α varies from 0 to 1. (It is interesting to note that the size-effect splitting of the bulklike $\bar{X}$ levels in the lower bulk band appears to be larger around $\alpha = 0.8$, rather than for the self-consistent potential.) Here the $(\bar{X}_3^+)_4$, $(\bar{X}_3^-)_3$ pair of surface states descends more or less steadily with the increase of α. On the other hand, the $(\bar{X}_1^{\pm})_4$ pair of surface states develops rather slowly for the first-half of α, and then it begins to descend rather rapidly for the second-half of α. Note that there is a domain of α for which both $\bar{X}_1$ and $\bar{X}_3$ surface states are well defined in the gap.

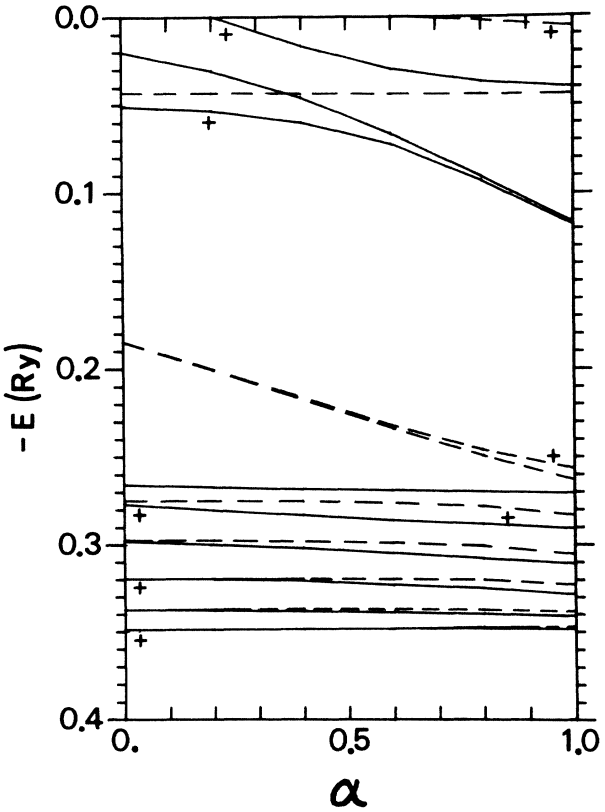

FIG. 7. $\bar{X}$ energy levels for a 13-layer Li (001) film as a function of the mixing parameter α, where $V(\alpha) = \alpha\, V(\text{self-consistent}) + (1-\alpha)V(\text{initial})$. $\bar{X}_3$ levels are given by dashed lines, $\bar{X}_1$ levels by solid lines, with the even z symmetry labeled by +.

In Fig. 8 we show the spatial behavior of the $\bar{X}_1^+$ surface state and for comparison that of the nearest bulklike $\bar{X}_1^+$ state below it in energy. The normalized surface state $(\bar{X}_1^+)_4$ reaches its maximum magnitude of 1.55 at $\bar{r}/a = (0, 0)$ and $z/\frac{1}{2}a \approx 6.4$, i.e., just outside the surface ion; for this $\bar{r}$, the magnitudes of the wave function's peaks are in the proportions 1.55:0.68:0.31:0.15. By contrast, the bulklike state $(\bar{X}_1^+)_3$ reaches its maximum magnitude 0.95 at $\bar{r}/a = (\frac{1}{4}, \frac{1}{2})$ and $z/\frac{1}{2}a = 3.0$, and the peaks show no marked pattern of surface localization. Note that since we have fixed the planar origin $\bar{r} = (0, 0)$ to coincide with an atom in the central plane, the surface state labeled by the irrep $\bar{X}_1$ here for the 13-layer film would also be labeled $\bar{X}_1$ for films of N_3 layers thickness for which $n_z = \frac{1}{2}(N_3 - 1)$ is even and the surface plane therefore an A plane. For films with a B surface plane (n_z odd) the same surface state will be labeled $\bar{X}_3$. In both cases the irreps correspond to wavefunctions with nodal planes normal to $\bar{k}$ and bisecting the line connecting nearest-neighbor atoms in the surface plane.

The status of the states $(\bar{X}_3^+)_4$, $(\bar{X}_3^-)_3$ is at present equivocal. Recall that the lower-$\bar{X}$ bulk band extends up to the level of the lowest $\bar{M}_5^+$ for in-

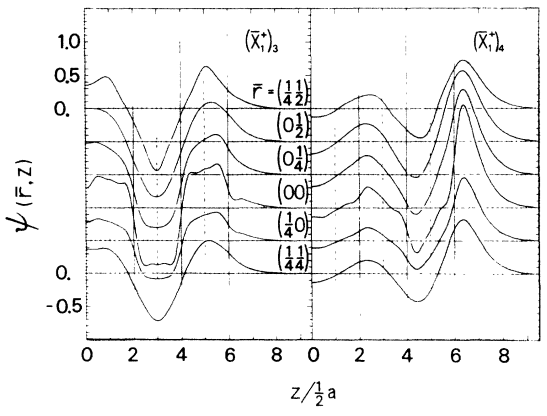

FIG. 8. Plot of the surface state $(\bar{X}_1^+)_4$ and bulk state $(\bar{X}_1^+)_3$ wave functions in a 13-layer Li (001) film for selected values of $\bar{r}$ (in units of a). (To save space, the curves are overlapped so that the $\psi = +0.5$ line for one curve coincides with the $\psi = 0$ line for the next one above.) The location of A planes is marked by solid vertical lines, that of B planes by dashed lines. The wave function is normalized to unity in a volume $2L \times a^2$.

finitely thick films. On this basis, the fact that in the self-consistent potential both these $\bar{X}_3$ states in the 13-layer film lie *below* the lowest-$\bar{M}_5^+$ level suggests that they lie in a bulk continuum of the same symmetry and could therefore be no more than surface resonances. On the other hand, in such thin films the bulk bands are not really continua, and there may be size effects which will allow such $\bar{X}_3$ states to rise above the lowest-$\bar{M}_5^+$ level in a thicker film. In the self-consistent 13-layer film these $\bar{X}_3$ states do appear to show some slight degree of surface localization. In Fig. 9 we show these wave functions for $\bar{r}/a = (\frac{1}{2}, \frac{1}{2})$ and from $z = -L$ to L. The even function has peak magnitudes in the proportions 0.78:0.71:0.62, which suggests some possible degree of surface localization. The forced node at the median plane in the odd function enhances the appearance of surface localization; its peak magnitudes have the proportions 0.97:0.76:0.42. For infinitely thick films, the surface-state pair of a given planar symmetry could be resolved into even and odd combinations of two surface states localized separately on each of the two surfaces. Following that line of thought, we also plot in Fig. 9 the normalized sum of the two $\bar{X}_3$ states in question. The sum function shows a striking localization on the right-hand face of the film; the peak magnitudes have the proportions 1.23:1.05:0.74:0.46:0.20:0.12. This result is very suggestive of the fact that these $\bar{X}_3$ states retain their surface character in the self-consistent potential; however, one should remember that a sum of an even and odd function having peaks at about the same places will show some reinforcement on one side and cancellation on the other. Further work will be required to settle the question of these $\bar{X}_3$ "surface" states.

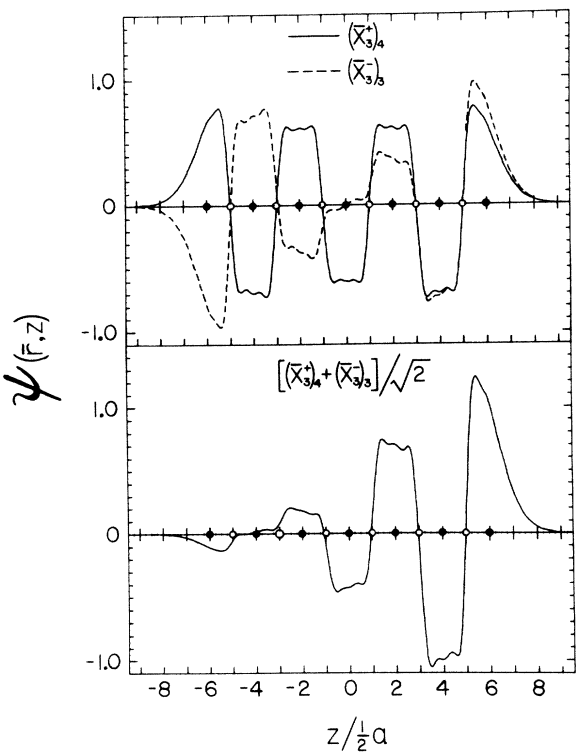

FIG. 9. Plot of the even $(\bar{X}_3^+)_4$ and odd $(\bar{X}_3^-)_3$ wave functions from the bottom of the $\bar{X}$ gap and their normalized sum for $\bar{r}/a = (\frac{1}{2}, \frac{1}{2})$. *A* planes are denoted by full circles, *B* planes by open circles. The wave functions are normalized to unity in a volume $2L \times a^2$.

To conclude, we return to the problem of the work function. Our result of 3.70 eV is 0.4 eV greater than the first-order lattice-corrected value of Lang and Kohn for the (001) face and 0.6 to 1.4 eV greater than the two polycrystalline experimental values cited by Lang and Kohn. Although the wide discrepancy between the two experimental values suggests that the experimental situation is less than satisfactory, in retrospect part of our large value for the work function is probably due to not making an optimal choice for $E_{\rm rep}$ in the atomic repulsive part of the pseudopotential. As stated in Sec. II, our calculation used a value $E_{\rm rep} = 4.4884$ Ry, which for the adopted lattice constant $a = 3.449$ Å gave $\Delta_N E = 0.209$ Ry for the N_1,-to-N_1 band gap in the bulk. For a plane-wave diagonal matrix element at the Fermi wavevector, we have $\langle \vec{K}_F | v_{\rm rep} | \vec{K}_F \rangle = E_{\rm rep} | \langle \vec{K}_F | \psi_{1s} \rangle |^2 = E_{\rm rep}\, 0.0676 = 0.3034$ Ry, at our adopted value of $E_{\rm rep}$. However, if we had chosen $E_{\rm rep}$ so as to match Ham's band gap $\Delta_N E = 0.219$ Ry (interpolated to $a = 3.449$ Å),[19] the value would be $E_{\rm rep} = 4.633$. We would then have $\langle \vec{K}_F | v_{\rm rep} | \vec{K}_F \rangle = 0.3132$ Ry, which represents an upward shift of 0.14 eV. If we had chosen $E_{\rm rep}$ so as to match Callaway's gap $\Delta_N E = 0.232$ Ry,[18] $E_{\rm rep} = 4.832$ and $\langle K_F | v_{\rm rep} | K_F \rangle = 0.3266$ Ry, which represents a shift upward of 0.32 eV. Thus a fit of our pseudopotential to Callaway's band gap would move our work function to within 0.1 eV of the preferred Lang-Kohn value and to within 0.3 eV of the larger of the two experimental values. The remainder of the discrepancy may be accounted for by the fact that our band width (both in the bulk and thin film) is 0.025 Ry less than Ham's[18] or Callaway's.[19] This appears to be caused by the fact that our core potential, taken from atomic structure calculations,[17] is stronger than the Seitz potential[19] which is constructed to fit atomic term values.

ACKNOWLEDGMENTS

We are grateful to the Computation Center, The University of Texas at Austin, for a generous

computer-time cost-sharing arrangement which made it possible to carry this work to completion. We have benefited in this work from our parallel collaboration with Dr. E. Caruthers on the work cited as Ref. 11; in particular, we acknowledge one of his suggestions that led to significant savings in computer time. One of us (G.P.A.) thanks Professor F. W. de Wette for his support during the preparation of this paper; he also thanks W. Jones and J. Jones for their hospitality during a crucial part of the writing of the paper.

APPENDIX: SUMMARY OF GROUP THEORY NOTATIONS FOR PLANAR SYMMETRY OF Li (001)

The character tables for the bcc (001) irreducible representations (irreps) are as follows:

C_{4v}(4mm)

$\bar{\Gamma}$, $\bar{M}$	E	$2\{C_4[001]\}$	$C_4^2[001]$	$2\{m(100)\}$	$2\{m(110)\}$	compatibility
$\bar{\Gamma}_1$, $\bar{M}_1$	1	1	1	1	1	$\bar{\Delta}_1$, $\bar{\Sigma}_1$, $\bar{Y}_1$
$\bar{\Gamma}_2$, $\bar{M}_2$	1	1	1	−1	−1	$\bar{\Delta}_2$, $\bar{\Sigma}_2$, $\bar{Y}_2$
$\bar{\Gamma}_3$, $\bar{M}_3$	1	−1	1	1	−1	$\bar{\Delta}_1$, $\bar{\Sigma}_2$, $\bar{Y}_1$
$\bar{\Gamma}_4$, $\bar{M}_4$	1	−1	1	−1	1	$\bar{\Delta}_2$, $\bar{\Sigma}_1$, $\bar{Y}_2$
$\bar{\Gamma}_5$, $\bar{M}_5$	2	0	−2	0	0	$\bar{\Delta}_1+\bar{\Delta}_2$, $\bar{\Sigma}_1+\bar{\Sigma}_2$, $\bar{Y}_1+\bar{Y}_2$

C_{2v}(2mm)

$\bar{X}(\frac{1}{2}, 0)$	E	$C_4^2[001]$	m(010)	m(100)	compatibility
$\bar{X}_1$	1	1	1	1	$\bar{\Delta}_1$, $\bar{Y}_1$
$\bar{X}_2$	1	1	−1	−1	$\bar{\Delta}_2$, $\bar{Y}_2$
$\bar{X}_3$	1	−1	1	−1	$\bar{\Delta}_1$, $\bar{Y}_2$
$\bar{X}_4$	1	−1	−1	1	$\bar{\Delta}_2$, $\bar{Y}_1$

C_{1h}(m)

$\bar{\Delta}(\xi 0)$ $\bar{Y}(\frac{1}{2}\xi)$ $\bar{\Sigma}(\xi\xi)$	E	m(010) m(100) m(1$\bar{1}$0)
$\bar{\Delta}_1$, $\bar{Y}_1$, $\bar{\Sigma}_1$	1	1
$\bar{\Delta}_2$, $\bar{Y}_2$, $\bar{\Sigma}_2$	1	−1

The summary of the unnormalized fully symmetric ($\bar{\Gamma}_1$ irrep of C_{4v}[4mm]) planar basis functions for the bcc (001) surface are shown below:

$$F_{\bar{G}_p}(\bar{r}) \equiv \sum_{\bar{G}}^{*\bar{G}_p} e^{i\bar{G}\cdot\bar{r}} ,$$

where $(m, n) \equiv \bar{G}_p a/2\pi$, and $C(x) \equiv \cos 2\pi x/a$. (In order of increasing magnitude of $\bar{G}$.)

$$F_{00}(\bar{r}) = 1,$$

$$F_{10}(\bar{r}) = 2[C(x)+C(y)] ,$$

$$F_{11}(\bar{r}) = 4C(x)C(y) ,$$

$$F_{20}(\bar{r}) = 2[C(2x)+C(2y)] ,$$

$$F_{21}(\bar{r}) = 4[C(2x)C(y)+C(x)C(2y)] ,$$

$$F_{22}(\bar{r}) = 4C(2x)C(2y) ,$$

$$F_{30}(\bar{r}) = 2[C(3x)+C(3y)] ,$$

$$F_{31}(\bar{r}) = 4[C(3x)C(y)+C(x)C(3y)] ,$$

$$F_{32}(\bar{r}) = 4[C(3x)C(2y)+C(2x)C(3y)] ,$$

$$F_{40}(\bar{r}) = 2[C(4x)+C(4y)] ,$$

$$F_{41}(\bar{r}) = 4[C(4x)C(y)+C(x)C(4y)] ,$$

$$F_{33}(\bar{r}) = 4C(3x)C(3y) .$$

The symmetrized two-dimensional plane-wave basis functions (S2DPW's) are shown by $\bar{\Gamma}$:$\bar{k}$

$= (0, 0)2\pi/a$. Only the $\bar{\Gamma}_1$ irrep has levels below the vacuum level for the Li (001) film. The basis functions are the normalized $F_{\bar{G}}(\bar{r})$ above: e.g.,

$$|\bar{\Gamma}_1(00)\rangle = |00\rangle = \alpha_0^{-1/2} F_{00} ,$$

$$|\bar{\Gamma}_1(10)\rangle = (4\alpha_0)^{-1/2} F_{10}, \text{ etc} .$$

$\bar{M}: \bar{k} = (\frac{1}{2}, \frac{1}{2})2\pi/a$. In the present application, the lowest levels belong to the two-dimensional irrep $\bar{M}_5$; basis functions for the first partner are given as follows, where $\beta_5 = 1$, $h = \frac{1}{2} + n$, $h' = \frac{1}{2} + n'$, n's integers:

$$|\bar{M}_5(hh)_{11}\rangle = \tfrac{1}{2}[(|hh\rangle - |\bar{h}\bar{h}\rangle) + \beta_5(|h\bar{h}\rangle - |\bar{h}h\rangle)] ,$$

$$|\bar{M}_5(hh')_{11}\rangle = \tfrac{1}{2}[(|hh'\rangle - |\bar{h}\bar{h}'\rangle) + \beta_5(|h\bar{h}'\rangle - |\bar{h}h'\rangle)] ,$$

$$|\bar{M}_5(hh')_{12}\rangle = \tfrac{1}{2}[(|h'h\rangle - |\bar{h}'\bar{h}\rangle) + \beta_5(|\bar{h}'\bar{h}\rangle - |\bar{h}'h\rangle)] .$$

If required, the second partner can be obtained by changing the row-column indices on the left as $11 \to 21$ and $12 \to 22$ and by changing on the right-hand side $\beta_5 \to -1$ $h \to h'$, and $h' \to h$. Partner one has nodes along the lines $x = 0$ and $y = \pm\frac{1}{2}a$; partner two, $y = 0$ and $x = \pm\frac{1}{2}a$.

Levels belonging to the $\bar{M}_1$ and $\bar{M}_4$ irreps exist above the Fermi level and below the vacuum. Their basis functions are given by the following, where $i = 1, 4$ and $\beta_1 = 1$, $\beta_4 = -1$:

$$|\bar{M}_i(hh)\rangle = \tfrac{1}{2}[(|hh\rangle + |\bar{h}\bar{h}\rangle) + \beta_i(|h\bar{h}\rangle + |\bar{h}h\rangle)] ,$$

$$|\bar{M}_i(hh')\rangle = 8^{-1/2}[(|hh'\rangle + |\bar{h}\bar{h}'\rangle + |h'h\rangle + |\bar{h}'\bar{h}\rangle) + \beta_i(|h\bar{h}'\rangle + |\bar{h}h'\rangle + |h'\bar{h}\rangle + |\bar{h}'\bar{h}\rangle)] .$$

$\bar{M}_1$ has nodal lines $x = \pm\frac{1}{2}a$ and $y = \pm\frac{1}{2}a$; $\bar{M}_4$, $x = 0$ and $y = 0$.

$\bar{\Delta}: \bar{k} = (\xi, 0)2\pi/a$, $0 < \xi < \frac{1}{2}$. For $h = \xi +$ integer, $n =$ integer $\neq 0$; $|\bar{\Delta}_1(h0)\rangle = |h0\rangle$; $|\bar{\Delta}_1(hn)\rangle = 2^{-1/2} \times [|hn\rangle + |h\bar{n}\rangle]$; $|\bar{\Delta}_2(hn)\rangle = 2^{-1/2}[|hn\rangle - |h\bar{n}\rangle]$. $\bar{\Delta}_1$ has no nodal lines; $\bar{\Delta}_2$, $y = \pm\frac{1}{2}a$.

$\bar{X}: \bar{k} = (\frac{1}{2}, 0)2\pi/a$. Only $\bar{X}_1$ and $\bar{X}_3$ levels lie below the vacuum level in Li (001); for $h = \frac{1}{2} +$ integer, $n =$ integer $\neq 0$, and $i = 1, 3$ with $\beta_1 = 1$, $\beta_3 = -1$, $|\bar{X}_i(h0)\rangle = 2^{-1/2}[|h0\rangle + \beta_i|\bar{h}0\rangle]$, and $|\bar{X}_i(hn)\rangle = \frac{1}{2}[(|hn\rangle + |h\bar{n}\rangle) + \beta_i(|\bar{h}\bar{n}\rangle + |\bar{h}\bar{n}\rangle)]$. $\bar{X}_1$ has nodal line $x = \pm\frac{1}{2}a$; $\bar{X}_3$, $x = 0$.

$\bar{Y}: \bar{k} = (\frac{1}{2}, \xi)2\pi/a$, $0 < \xi < \frac{1}{2}$. For $h = \frac{1}{2} + n$, $h' = \frac{1}{2} + n'$ (n, n' integers which may be equal) and $\beta_1 = 1$, $\beta_2 = -1$, $|\bar{Y}_i(h, h')\rangle = 2^{-1/2}[|hh'\rangle + \beta_i|\bar{h}h'\rangle]$. $\bar{Y}_1$ has nodal line $x = \pm\frac{1}{2}a$; $\bar{Y}_2$, $x = 0$.

$\bar{\Sigma}: \bar{k} = (\xi, \xi)2\pi/a$, $0 < \xi < \frac{1}{2}$. For $h = \xi + n$, $h' = \xi + n'$ (n, n' integers and $n \neq n'$), $|\bar{\Sigma}_1(hh)\rangle = |hh\rangle$, $|\bar{\Sigma}_1(hh')\rangle = 2^{-1/2}[|hh'\rangle + |h'h\rangle]$; $|\bar{\Sigma}_2(hh')\rangle = 2^{-1/2} \times [|hh'\rangle - |h'h\rangle]$. $\bar{\Sigma}_1$ has no nodal lines; $\bar{\Sigma}_2$, $x = y$.

---

*Research supported by the U. S. Air Force Office of Scientific Research under Grant No. AF-AFOSR-72-2308 and by the National Science Foundation under Grant No. GH-40371.

[1]G. P. Alldredge and L. Kleinman, Phys. Rev. Lett. 28, 1264 (1972).

[2](a) For monatomic crystals, see, e.g., R. E. Allen, G. P. Alldredge, and F. W. de Wette, Phys. Rev. B 4, 1648, 1661 (1971), and references therein; (b) for ionic crystals, see, e.g., T. S. Chen, G. P. Alldredge, and F. W. de Wette, Solid State Commun. 10, 941 (1972), and references therein.

[3]This statement must be qualified in the case of surface-localized excitations whose localization depth becomes infinite as the wave vector approaches the origin of the SBZ, such as the Rayleigh surface waves. However, even these excitations can be resolved when their localization depths become smaller than the half thickness of the film, and, for films of a dozen or more layers, this frequently holds over the greater part of the two-dimensional phase space represented by the SBZ.

[4]J. A. Appelbaum and D. R. Hamann, Phys. Rev. B 6, 2166 (1972).

[5]There have been a few recent self-consistent surface calculations for simple models: A. J. Bennett and C. B. Duke, Phys. Rev. 188, 1060 (1969), an scf calculation for a one-dimensional Kronig-Penney model; H. Büttner and E. Gerlach, Surf. Sci. 32, 687 (1972), Fermi-Thomas screening of Shockley surface states in a simple tight-binding approximation (TBA) for a diatomic one-dimensional chain; H. Stoll and H. Preuss, Phys. Status Solidi B 53, 519 (1972), full Hartree-Fock calculations for small aggregates of Li and Be atoms, including linear chains of up to ten atoms; G. Allan and P. Lenglart, Surf. Sci. 30, 641 (1972), uses Friedel sum rule to obtain self-consistency in a simple TBA model for the simple cubic (001), (110), (111), the bcc (001), (110), and the fcc (001) surfaces; C. W. Deutsche, Phys. Rev. B 7, 1524 (1973), scf calculation for a one-dimensional model of a diatomic ionic semiconductor.

[6]N. D. Lang, in *Solid State Physics*, edited by H. Ehrenreich, F. Seitz, and D. Turnbull (Academic, New York, 1973), Vol. 28, p. 225.

[7](a) S. G. Davison and J. D. Levine, in *Solid State Physics*, edited by H. Ehrenreich, F. Seitz, and D. Turnbull (Academic, New York, 1970), Vol. 25, p. 1; (b) J. D. Levine and P. Mark, Phys. Rev. 182, 926 (1969).

[8](a) N. D. Lang, Solid State Commun. 7, 1047 (1969); (b) N. D. Lang and W. Kohn, Phys. Rev. B 1, 4555 (1970); (c) 3, 1215 (1971).

[9]J. A. Appelbaum and D. R. Hamann, Phys. Rev. Lett. 31, 106 (1973).

[10]For extensive discussion of the importance of nonlocality in pseudopotentials see, e.g., M. L. Cohen and V. Heine, in Ref. 7(a), Vol. 24, p. 38.

[11]E. Caruthers, L. Kleinman, and G. P. Alldredge, (a) Phys. Rev. B 8, 4570 (1973); (b) Phys. Rev. B 9, 3325 (1974); (c) Phys. Rev. B 9, 3330 (1974); (d) Phys. Rev. B (to be published).

[12]D. S. Boudreaux, Surf. Sci. 28, 344 (1971).
[13]B. I. Lundquist, K. Mountfield, and J. W. Wilkins, Solid State Commun. 10, 383 (1972).
[14]See, e.g., A. A. Cottey, J. Phys. C 6, 2446 (1973), and references therein.
[15]We use the term "selvage" as proposed by E. A. Wood, J. Appl. Phys. 35, 1306 (1964), to denote the region over which periodicity normal to the surface has disappeared. For metallic electron problems it is useful to further divide the selvage into the inner selvage—that region interior to a nominal surface plane such as the jellium edge—and the outer selvage—that region external to the nominal surface plane. In AK and Ref. 11 the word "selvage" is frequently used specifically for the outer selvage.
[16]Since our Hamiltonian matrices are real symmetric in the basis set adopted, we used the Givens-Householder method for diagonalizing such matrices. The specific form used is the highly optimized routine SPEED written by Peter K. Bischof (University of Texas at Austin, 1972) in the CDC6600 assembly language Compass. SPEED is based on the Fortran subroutine GIVENS written originally by Franklin Prosser (Indiana University, 1967) and optimized in Fortran for the CDC6600 by T. L. Hardgrave (UT-Austin, 1971).
[17]F. Herman and S. Skillman, *Atomic Structure Calculations* (Prentice-Hall, Englewood Clifs, N.J., 1963).
[18]J. Callaway, Phys. Rev. 124, 1824 (1961); 131, 2839(E) (1963).
[19]F. S. Ham, Phys. Rev. 128, 82, 2524 (1962).
[20]P. A. Anderson, Phys. Rev. 75, 1205 (1949). However, J. C. Riviere [in *Solid State Surface Science*, edited by M. Green (Dekker, New York, 1969), Vol. 1, p. 179] has revised Anderson's value of 2.49 eV downward to 2.32 eV in light of a subsequent determination of a standard value for the work function of polycrystalline tungsten. See also Ref. 8(c) for discussion of the lithium work function values.
[21]In common with AH and others, in this paper we work solely with the pseudocharge density. More detailed work would require correction for the orthogonalization hole (see, e.g. Ref. 10 and the article by V. Heine and D. Weaire in the same volume). A rough estimate of the size of this effect is given by the ratio of volumes of the core and atomic spheres: $(r_{\text{core}}/r_s)^3 \approx 0.06$. In the present case of lithium, however, the absence of p-like components in the repulsive potential means that the effect of the orthogonality hole is even smaller than this rough estimate suggests.
[22]Note that this cosine-series expansion is that of functions that are periodic under $z \to z + 2L$, in contrast to the basis functions of Eq. (2.2) which only vanish at $z = \pm L$. This series is generated by products of the functions (2.2): $\langle \sigma k_z | z \rangle \times \langle z | \sigma k_{z'} \rangle = L^{-1}[\cos(k_z - k_{z'})z + \sigma \cos(k_z + k_{z'})z]$. Also note that for $q \neq 0$, the q components of this cosine series are twice the value of the q components of the equivalent exponential series.
[23]Although for q too small the right-hand side of Eq. (2.16) becomes numerically unstable because of the truncation and rounding errors, with the 60 bit single precision word length of the CDC6600 there is an accessible range of q sufficiently close to zero that it yields V_{00}^{Coul} to seven significant figures. For computers of less precision, $V_{0,q}^{\text{Coul}}$ can be evaluated as

$$V_{00}^{\text{Coul}} = -\frac{4\pi a}{\alpha_0}[\langle z^2 \rangle_{\bar{0}} - \langle l_3^2 \rangle_{\bar{0}}]$$

where

$$\langle z^2 \rangle_{\bar{0}} \equiv \frac{a}{2L}\int_{-L}^{L}\left(\frac{z}{a}\right)^2 \frac{\rho_{\bar{0}}(z)a^3 dz}{a}$$

and

$$\langle l_3^2 \rangle_{\bar{0}} \equiv \left(\frac{a}{2L}\right) 2 \sum_{l_3=1}^{n_z} \{\tfrac{1}{2}[l_3 + s(l_3)]\}^2.$$

[24]Output potentials are always worse than input potentials in the sense that a potential consisting of a mixture of the input and output potentials is much less self-consistent than the original input potential. (See Sec. II.) Therefore we do not use the output potential of the final iteration except as a check on the self-consistency of the input.
[25]R. Smoluchowski, Phys. Rev. 60, 661 (1941).